Scrutiny of the Failure of Lipid Membranes as a Function of Headgroups, Chain Length, and Lamellarity Measured by Scanning Force Microscopy

Stephanie Künneke, Daniel Krüger, and Andreas Janshoff
Johannes Gutenberg Universität Mainz, Institut für Physikalische Chemie, 55128 Mainz, Germany

ABSTRACT A fast, quantitative, and unambiguous screening of material properties of biomembranes using scanning force microscopy in pulsed force mode on lipid membranes is presented. The spatially resolved study of breakthrough force, breakthrough distance, adhesion, stiffness, and topography of lipid membranes as determined simultaneously by digitalized pulsed force mode provides new insight into the structure-function relationship of model membranes, which are systematically analyzed by varying chain length, lipid headgroup, and lamellarity. For this purpose, a novel unbiased analysis method is presented. A strong correlation between adhesion and breakthrough events is found on lipid bilayers and multilayers and discussed in terms of structural stability and chemical and physical interactions. Our findings indicate that multilamellar 1-palmitoyl-2-oleoyl-*sn*-glycero-3-phosphoserine is mechanically strengthened with respect to material failure by calcium ions in solution.

INTRODUCTION

Biological membranes mainly consist of lipids, steroids, and proteins. The ultimate function of lipids with respect to the structure of biomembranes lies in their ability to self-organize into specific supramolecular aggregates—an attribute conferred by the inherent amphiphilic nature of this diverse class of biomolecules. Lipid bilayers not only serve as a host matrix for proteins but also exhibit unique electrical and mechanical properties providing the basis for living organisms. The structure and function of biomembranes has generated an enormous interest among researchers in the field of biophysics and bioanalytical chemistry. Among the different model systems mimicking the situation of the native membrane solid supported lipid bilayers are the most versatile ones for studying physical properties, lateral organization, and protein-lipid interaction on a small scale with spatially resolved techniques. In particular, scanning probe techniques such as the scanning force microscope (SFM) emerging from its ancestor the scanning tunneling microscope provides a means to image various properties of thin films beyond topography comprising mechanical and electrical parameters on a molecular level. Moreover, the ability to use the SFM in an aqueous solution has added to its applicability for studying biological objects under almost native conditions. Among the vast amount of local probe techniques, scanning force microscopy is the most versatile technique to investigate the structural organization of lipids, lipid-protein complexes on flat surfaces, as well as the mechanical properties of lipid membranes.

The latter are obtained from force curve studies (Cappella and Dietler, 1999; Janshoff et al., 2000) where the deflection of the cantilever is measured as a function of piezo displacement. This work presents a quantitative investigation of the correlation between adhesion and elasticity of different lipid membranes by analyzing material-dependent breakthrough events, i.e., failure of the membrane, describing the penetration of the SFM tip through the lipid bilayer as shown in Scheme 1. Fig. 1 illustrates force curves measured with a conventional SFM setup (*left*) and with the pulsed force mode (PFM) (*right*) both showing breakthrough events occurring as instabilities in the contact regime. Several groups (Dufrene et al., 1997, 1998; Mueller et al., 1999; 2000) reported on material-dependent breakthrough events on different lipid bilayers with regard to imaging contrast mechanisms (Schneider et al., 2000) or the activation process of the penetration of the SFM tip through the lipid bilayer (Butt and Franz, 2002; Loi et al., 2002; Franz et al., 2002), respectively. A quantitative analysis of the correlation of adhesive and elastic properties and their dependence on the lipid headgroup, chain length, and the membrane lamellarity was still missing and is presented in this work.

In contrast to earlier investigations, the presented evaluations of breakthrough force, breakthrough distance, adhesion, and stiffness are based on SFM measurements using the pulsed force mode (Rosa-Zeiser et al., 1997; Miyatani et al., 1997, 1998; Krotil et al., 1999). The major advantage of the PFM compared to conventional static force curve sampling is the possibility of obtaining the same information at much higher data rates without the need for any change in the SFM instrumental design. Especially for quantitative mechanical investigations high information throughput is desirable because the distribution of rupture force contains valuable information about the mechanism of hole forming (Butt and Franz, 2002).

Although the usage of the pulsed force mode for investigations of mechanical lipid membrane properties is obviously consistent with the need for large statistics required for a quantitative analysis of this type, an essential

Submitted May 30, 2003, and accepted for publication October 30, 2003.

Address reprint requests to Andreas Janshoff, Johannes Gutenberg Universität Mainz, Institut für Physikalische Chemie, Welder-Weg 11, 55128 Mainz, Germany. E-mail: janshoff@mail.uni-mainz.de.

0006-3495/04/03/1545/09 $2.00

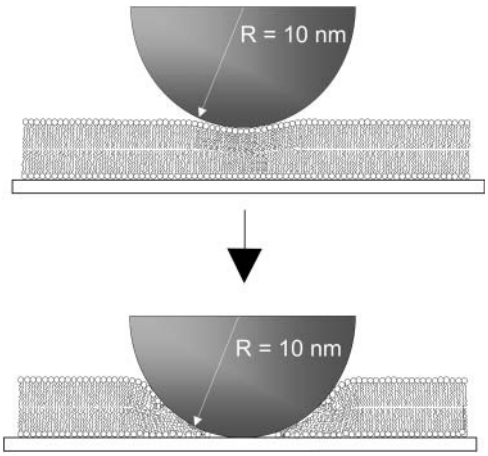

SCHEME 1 Schematic drawing of a SFM tip penetrating a solid supported lipid bilayer.

prerequisite is the development of automated analysis methods. We present an automated analysis scheme for the detection of breakthrough events, which is based on a multiparameter cluster analysis and makes the potentially biased single contact curve evaluations obsolete. At the same time the automated analysis keeps the advantage of the rapid analysis scheme as provided by the usage of the pulsed force mode.

EXPERIMENTAL SECTION

Small unilamellar vesicles of 1-palmitoyl-2-oleoyl-*sn*-glycero-3-phosphoserine (POPS), 1-palmitoyl-2-oleoyl-*sn*-glycero-3-phosphocholine (POPC), 1,2-dimyristoyl-*sn*-glycero-3-phosphocholine (DMPC), 1,2-dimyristoyl-*sn*-glycero-3-phosphoserine (DMPS), and 1,2-dipalmitoyl-*sn*-glycero-3-phosphoserine (DPPS) (Avanti Polar Lipids, Alabaster, AL) were prepared by the extrusion method using two stacked polycarbonate membranes with an average pore diameter of 100 nm. An amount of 200 μl of each vesicle suspension (POPS, DMPS, DPPS 1 mg/ml; POPC, DMPC 0.2 mg/ml) was incubated overnight on freshly cleaved mica at 4°C. Before heating for 45 min at 60°C the samples were rinsed with buffer to remove vesicles not adsorbed to mica. Subsequent to cooling the samples to room temperature they were rinsed with buffer again. All experiments were performed in 2 mM $CaCl_2$, 150 mM NaCl, 10 mM Tris/HCl buffered at pH = 7.4.

Experiments were carried out in aqueous solutions using a commercial scanning force microscope (Dimension 3100 with Nanoscope IIIa+A/D controller, Veeco Digital Instruments, Santa Barbara, CA) extended with a pulsed force box (WITec GmbH, Ulm, Germany) and silicon nitride cantilevers (OMCL-TR400PSA, Olympus, Japan).

Measurements of the thermal power spectrum densities yielded individual spring constants of the cantilevers from 0.07 to 0.09 N/m (Butt and Jaschke, 1995). The tip radii were estimated by deconvolution of images of a tip calibration grid TGT01 (Anfatec, Germany). Compared measurements were carried out using the same SFM tip. A PC card (NI 5911, National Instruments USA, Austin, TX) was used to digitalize the PFM traces (1000–5000 per experiment) for the force curve mapping. ''Substract Baseline'' was switched to ''On'' at the PFM box for all measurements.

RESULTS AND DISCUSSION

General remarks on PFM in water

Although the usage of high-speed force curve sampling modes like PFM is straightforward with the cantilever operated in gaseous environment the operation in liquids requires a deeper understanding of the governing mechanisms. The critical parameter, which causes this difference in the two media, is the cantilever damping being drastically increased in liquid phases (e.g., the dynamic viscosity of water is ~50 times higher than for dry air). At these magnitudes of damping substantial phase lags between the driving force and the measured force can appear, which may lead to a possible misinterpretation of the adhesion data. As our scope is a quantitative analysis, we initiated the investigations with simulations of the PFM under liquid conditions as inherently required for the model membranes (S. Krüger, D. Krüger, and A. Janshoff, unpublished data). The performed simulations enabled us to understand which system information is extractable and to optimize the operating parameters regarding speed and stability. A typical effect is the formation of a second force maximum on the left-hand side of the force maximum in the contact regime at about one-

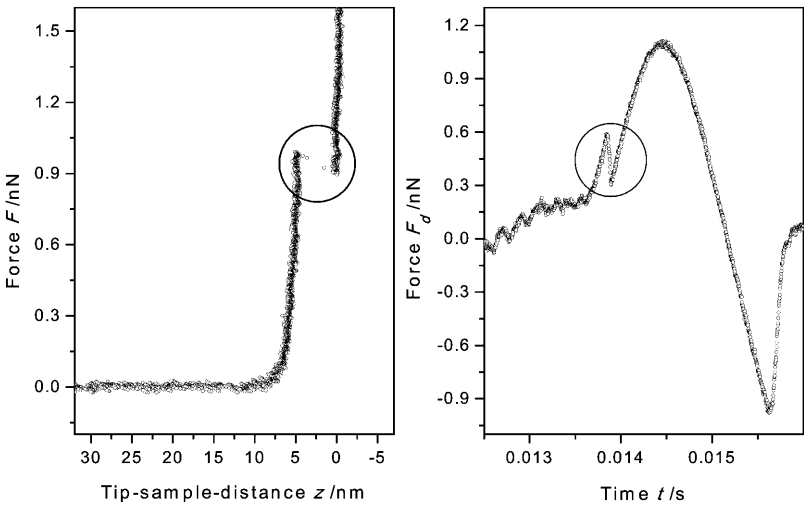

FIGURE 1 Force curves obtained by conventional force microscopy (*left*) and by pulsed force microscopy (*right*) on POPS bilayers systems. Both graphs exhibit breakthrough events in the contact regime.

half of the driving period that is caused by the large hydrodynamic damping. Hydrodynamic damping affects the SFM cantilever at the maximum driving velocity. By choosing smaller set points for the maximum force trigger the hydrodynamic force maximum can easily become larger than the contact maximum force. This is no major hindrance in a quantitative exploration of the PFM if the contact onset point is still clearly identifiable. On the other hand, the same mechanism is responsible for the hydrodynamic force on the retraction away from the sample that might obscure the correct point of detachment from the surface. Hence, in the experiments presented here we followed the approach to reduce hydrodynamic damping to acceptable magnitudes by decreasing both the driving amplitude and frequency. Decreasing the amplitude is limited by the need to overcome maximum adhesion on the sample and to exert sufficient load for the observance of the mechanical instabilities on thin film systems. In principle the driving frequency can be reduced arbitrarily, however, the intention is to keep the advantage of the PFM as a rapid acquisition mode. We find that amplitudes of 7–12% together with driving frequencies f_d of 100–300 Hz satisfy the latter needs and will at the same time reduce hydrodynamic damping sufficiently to generate reliable adhesion data.

Multiparameter analysis method

Due to the high data rates (~100 force curves/s) the data analysis has been automated. Our focus on this study lies on the detection of breakthrough events within a single period of the PFM force curve. As the force required for such a mechanical instability of the lipid membrane is stochastic, the breakthrough will neither appear at specific points of the trace nor will it be safe to assume that it takes place in every period up to the given force maximum. In practice, we find that a semiautomated analysis based on an automated preprocessing step followed by a manual data cluster analysis gives the most reliable results in detecting the breakthrough forces, breakthrough distances, and, with some limitations, also the Young modulus of the film as evaluated before the breakthrough point. The first preprocessing step is based on a line fit over a time range Δt_l (l = line) being a fraction of the driving period ΔT. The line fit is performed over the full accessible range of every period (t within $\Delta t_l/2$ to $\Delta T - \Delta t_l/2$) such that one obtains for every time t functions for the slope $a(t)$, the offset $b(t)$, and the line fit square deviation $\chi^2(t)$. Starting from a predefined time t_0 before the breakthrough up to the time of the force maximum $t(F_{max})$, the maximum of the function $f_b(t) = \chi^2(t)(da(t)/dt)$ is used to detect the end t_e of a potential breakthrough. Therein both the absolute values of $da(t)/dt$ as well as $\chi^2(t)$ effectively act as edge detectors while at the same time the line fitting efficiently smoothes the curves without obscuring information on edge positions. The onset of the breakthrough t_s (s = start) is then derived from the maximum of $f_b(t)$ with t lying between t_0 and t_e. Subsequently the breakthrough length d can be evaluated from $d = y_s(t_s) - y_e(t_s)$, with $y_s(t)$ and $y_e(t)$ being the regression lines 1 and 2 as shown in Scheme 2 with a local minimum of $\chi^2(t)$ before the breakthrough onset and after the breakthrough end. Additionally the corresponding slopes a_s and a_e provide information on the contact stiffness before the breakthrough and after the breakthrough. Based on the relation $1/S = 1/k_C + 1/k_S$ between a force gradient S, the cantilever stiffness k_C and sample contact stiffness k_S one obtains:

$$k_{ss} = \frac{a_s k_C}{a_e(1 + q_k) - a_s}, \quad (1)$$

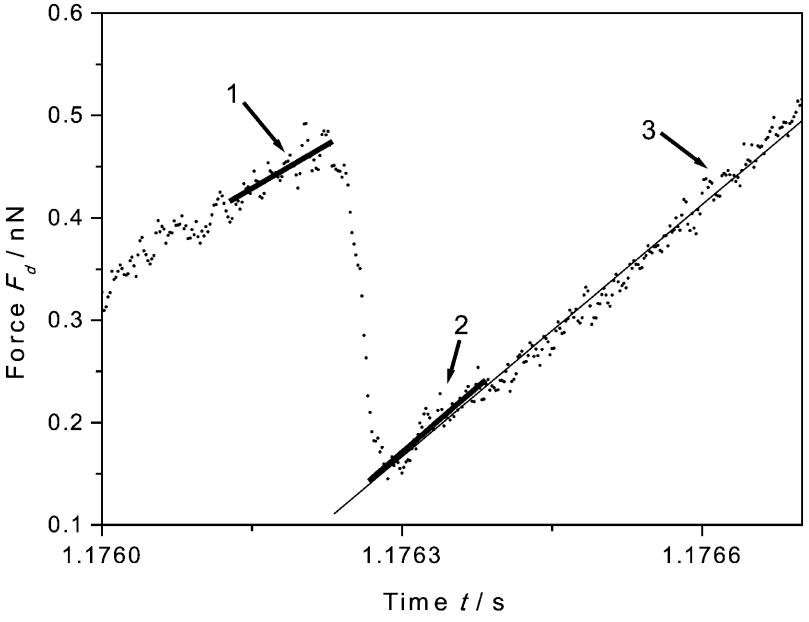

SCHEME 2 The breakthrough lengths, breakthrough distances, and the sample stiffness are deduced from the regression lines before the breakthrough (*1*), directly after the breakthrough (*2*), and in contact with the mica substrate (*3*).

with k_{ss} being the sample contact stiffness before breakthrough and q_k being the relative stiffness of the cantilever and the contact stiffness k_{se} after the breakthrough ($q_k = k_c/k_{se}$). When the tip touches the hard mica surface, hard with respect to the membrane, directly after the breakthrough ($q_k \cong 0$) Eq. 1 can be used to calculate the sample contact stiffness k_{ss} before breakthrough without explicitly calibrating the piezo movement or the SFM sensitivity (Eq. 1 holds for slopes as obtained in arbitrary units, i.e., mV). The contact stiffness k_S might be roughly related to the Young modulus E of the sample related by Sneddon (1965):

$$k_S = \frac{2RE}{(1-\nu^2)}. \quad (2)$$

R is the contact radius and ν the Poisson ratio.

The breakthrough events suggested by the automated detection in every PFM period have to be separated in a second manual postprocessing step to distinguish between noise and correct detections. This is easily performed by manually setting threshold values for the breakthrough length or breakthrough force.

Influence of membrane lamellarity

Here we present data on the dependence of membrane stability on the lamellarity of 1-palmitoyl-2-oleoyl-*sn*-glycero-3-phosphoserine (POPS) membranes measured by PFM microscopy. Phosphatidylserine is a major anionic lipid component in mammalian cells especially found in the inner leaflet of the plasmamembrane (Mattai et al., 1989). The liquid-crystalline-gel phase transition temperature of POPS is Ca^{2+} dependent and lies between 14 and 15°C for solutions containing 2 mM Ca^{2+} (Demel et al., 1987). After spreading and fusion of POPS vesicles on mica SFM images reveal that bilayer regions coexist with two lamellae-multilayer regions.

Topography, stiffness, and maximum adhesion images as obtained from the standard PFM imaging of POPS are shown in Fig. 2. Both bilayer and multilayer domains show the same stiffness contrast (Fig. 2 *B*) and are softer (*darker regions*) than the mica substrate (*lighter regions*). The adhesion measurement (Fig. 2 *C*) reveals the POPS bilayer to be highly adhesive (*light*) compared to the multilayer segment and the mica substrate both, showing minor adhesion (*dark*).

Finding substantially differing adhesion between multilayer and bilayer is surprising as both domains expose the same type of headgroup toward the tip. Although it is known from monolayer systems facing the chains toward the SFM tip, that the adhesion of thin films with the same headgroup can vary with the stiffness of the system (Barger et al., 1996; Koleske et al., 1997), here we essentially observe the same stiffness on both the multi- and bilayers such that this effect can be excluded.

In contrast, the analysis of the breakthrough behavior of the POPS system reveals a strong correlation between breakthrough events and adhesion. Typical PFM force curves

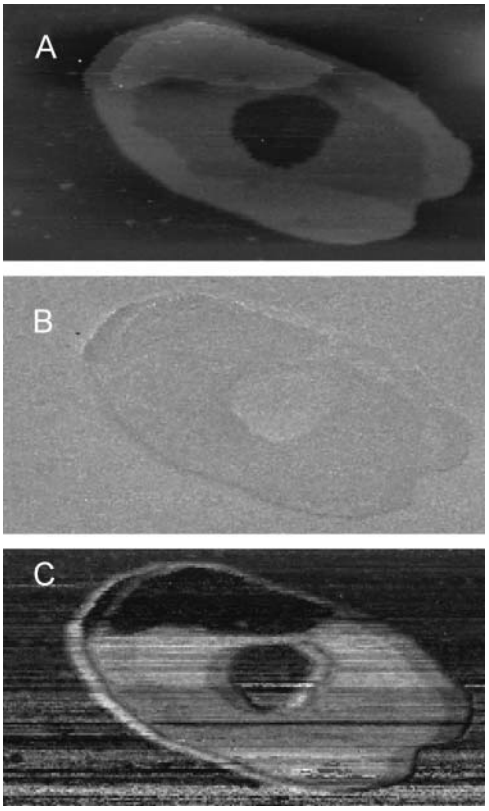

FIGURE 2 Scanning force microscopy images (300 nm × 600 nm; PFM mode; $k_c = 0.08$ N/m; $f_d = 300$ Hz; $A_d = 1.28$ nN) showing (*A*) the topography of a POPS lipid membrane patch on mica (total height 20 nm) and the corresponding stiffness (*B*) and adhesion (*C*) images. Note that the stiffness trigger is set to a low force to avoid vanishing contrasts from postbreakthrough triggering. The membrane exhibits bilayer and double bilayer regions as deduced from a height analysis of the topography image (data not shown).

measured on POPS bilayer and multilayer regions are depicted in Fig. 3. Although POPS on mica shows very clear breakthrough events on the bilayer domains and strong adhesion values, no breakthrough and small adhesion values were observed on double bilayer regions. The correlation between breakthrough distance, breakthrough force, and adhesion force is demonstrated in the cluster representation displayed in Fig. 4 as obtained from the automated detection. The graph shows two distinct cluster regions easily enabling the separation of false detections and actual breakthrough events. Obviously, the smaller cluster containing data points with negative breakthrough distances can be attributed to the noise detections, meaning that no breakthrough events were observed in the specific approach cycles. Interestingly, high adhesion force values are only observed in the cases where the tip broke through the lipid membrane whereas the maximum adhesion force of the double bilayer is rather small as indicated by the histogram analysis (Fig. 5). This is indicative of a tip interaction with the chains being much stronger than interaction with the bilayer headgroups and an increased contact area. However, it might also be possible

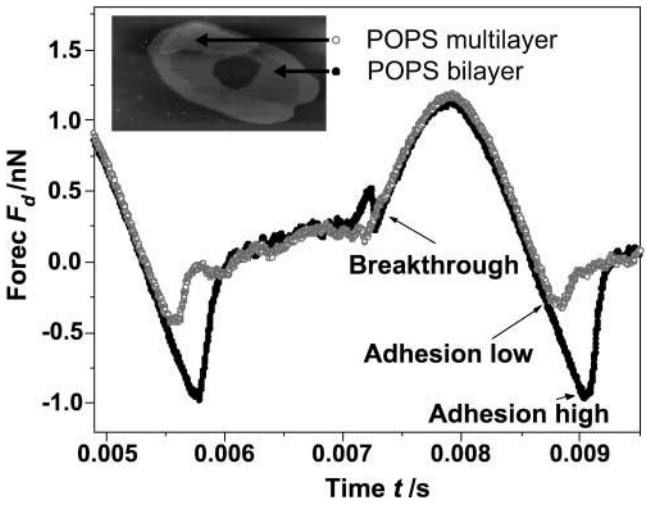

FIGURE 3 Typical PFM traces showing force versus time corresponding to the piezo displacement. The force curve measured on the POPS bilayer (●) exhibits the lipid breakthrough event in the contact regime and an adhesion value of 0.97 nN, whereas the POPS double bilayer (○) shows only an adhesion value of 0.35 nN. No breakthrough is observed on the POPS multilayer under the same maximum load.

that contact of the tip with the mica surface after the breakthrough took place is responsible for the increased adhesion after failure of the membrane. Either way, membrane rupture yields in increasing adhesion between tip and sample.

The strict correlation between adhesion and breakthrough event is indicative for a strong stabilization of the PS lamellae probably due to the formation of a cochleate phase in a PS multilayer system, which is well known to form in the presence of Ca^{2+} (Feigenson, 1986; Casal et al., 1987; Roux and Bloom, 1991). The low-affinity binding of Ca^{2+} to the single bilayer being about six orders of magnitude weaker than the binding between the PS lamellae (Feigenson, 1989) leads to destabilization and there is no penetration of the SFM tip through the multilayer at the forces applied. These findings have strong implications for the understanding of membrane-membrane contacts as they occur within cells as the initial reaction of exocytosis.

The correlation between the breakthrough forces and the breakthrough distances and a histogram analysis of both parameters for the POPS bilayer are shown in Fig. 6. The distances (Fig. 6 *B*) correspond very well to the expected bilayer height, when considering the indentation of the SFM tip and the additional water layer sandwiched between the film and the substrate.

As far as the yield forces are concerned, Butt and Franz recently introduced a theoretical framework based on the kinetic model of Evans for force supported rupture of molecular linkages that allows extracting further information from the yield force distribution (Butt and Franz, 2002). The authors describe the film rupture as an activated process in which the activation barrier is reduced due to the fact that the initial free energy is increased as the tip exerts pressure on the membrane. The authors introduce basically two concepts, one based on a so-called continuum nucleation model and the other on a molecular model to find an expression for the activation barrier for the failure of a thin film. For the continuum model the following probability density function $\Xi(F)$ was found:

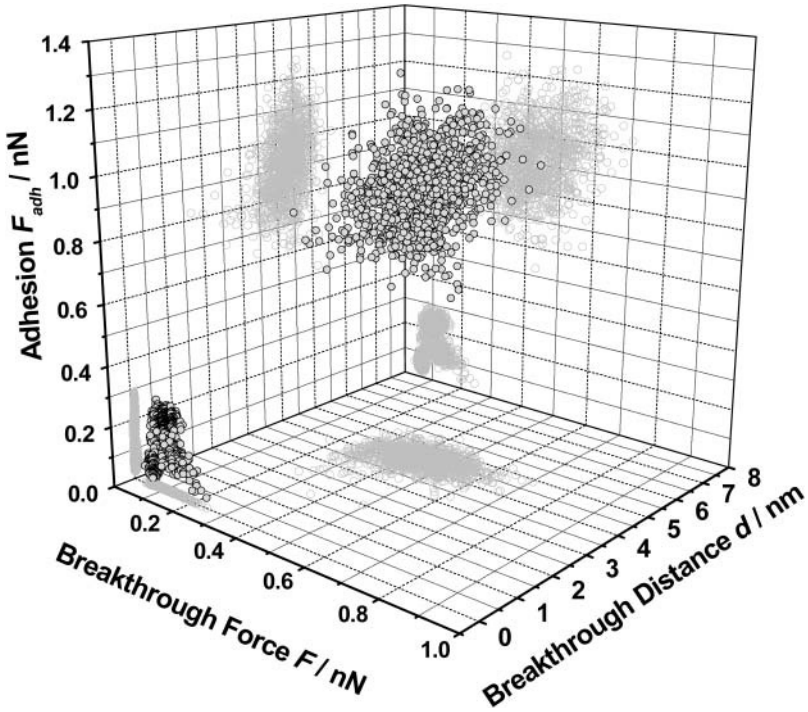

FIGURE 4 Three-dimensional cluster analysis of breakthrough events on a POPS bilayer/POPS multilayer/mica system as obtained from the automated preprocessing. Orthogonal projections of the maximum adhesion force, the breakthrough force, and breakthrough distance as obtained from the same PFM periods visualize the cluster extensions. The driving frequency was set to $f_d = 300$ Hz, the driving amplitude to $A_0 = 1.28$ nN.

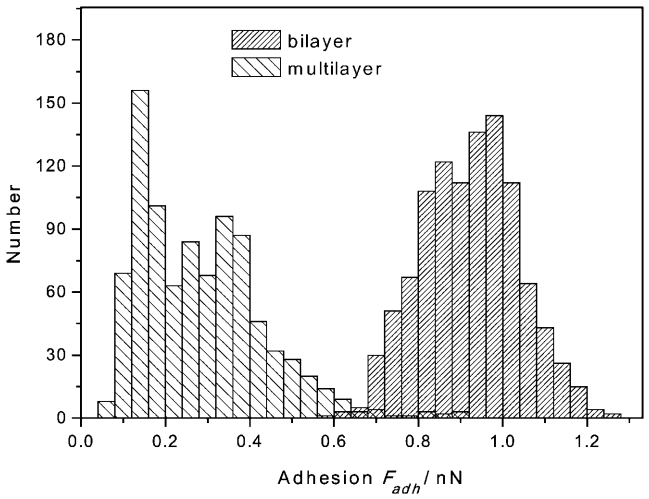

FIGURE 5 Histogram analysis of the adhesion forces on POPS bilayer regions (*thin-striped bar*) and POPS double bilayer regions (*wide-striped bar*). The high values of the adhesion force on POPS bilayers (mean adhesion $F_{adh} = 0.92 \pm 0.11$ nN) are well separated from the small adhesion values from POPS double bilayers (mean adhesion $F_{adh} = 0.29 \pm 0.15$ nN).

$$\Xi(F) = \left| \frac{d}{dF} \left(1 - \exp\left(-\frac{A}{kv} \int_{2\pi Rs}^{F} \exp\left(\frac{-2\pi^2 \Gamma^2 R}{(F - 2\pi Rs) k_b T} \right) dF \right) \right) \right|. \quad (3)$$

A denotes the frequency factor limited by the resonance frequency of the cantilever (10^4 Hz), Γ is the line tension, s the spreading factor that represents a measure of how strong the bilayer is attached to the substrate. R is the tip radius (25 nm) and F the applied load force.

For the POPS bilayer we obtained a low line tension Γ of 10^{-12} N and spreading coefficient of 0.0015 N/m indicative of a weak attachment to the surface. These findings are in good agreement with the work of Loi et al. (2002) who also found a lower line tension and spreading factor for negatively charged DOPS bilayers compared to positively charged DOTAP bilayers.

Employing the simplified molecular model characterized by the following two-parameter distribution function

$$\Xi(F) = \left| \frac{d}{dF} \left(\exp\left(-\frac{k_0 F_t}{kv} \left(\exp\left(\frac{F}{F_t} \right) - 1 \right) \right) \right) \right|, \quad (4)$$

with k_o, the rate constant in the absence of external force, $F_t = 4\pi h R k_b T / V$, with V, the activation volume, and h the unit area (Loi et al., 2002). k_o was determined to $(38 \pm 8)\ s^{-1}$ and $F_t = (0.08 \pm 0.004)$ N. The average yield force was 0.4 N as approximated by the maximum of the distribution functions (Eqs. 3 and 4).

In other studies occasionally multiple breakthrough events were observed (Franz et al., 2002; Loi et al., 2002). The authors found that the breakthrough distances do not agree with the thickness of one lipid bilayer. Mueller et al. (1999) report on the occurrence of a jump-in distance of 7–8 nm corresponding to a penetration of both layers in one jump, respectively. In contrast, the breakthrough distances we observed in our study on POPS fit very well to a single bilayer and no multiple jumps of the tip were found. Taking into account the electrostatic repulsion between the tip and the lipid bilayer, both being negatively charged, coverage of the silicon nitride tip with lipid molecules is not favored.

Besides our findings that support that measurements of a repeatable, material-dependent breakthrough force are possible, other authors also report that characteristic jumps that did not change over time can be observed (Schneider et al., 2000; Mueller et al., 2000). Our own measurements of POPS bilayers do not show any change, either in breakthrough distance, adhesion force, or yield force with time during the scanning procedure. This is not surprising because we scan while we collect the PFM curves at

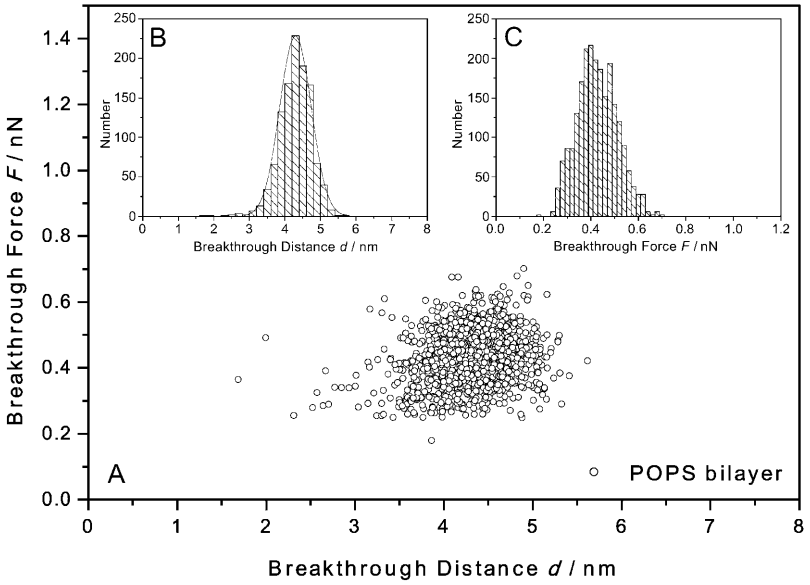

FIGURE 6 Breakthrough force as a function of breakthrough distance (*A*) for a POPS bilayer and histogram analysis of the breakthrough distances (*inset B*) and the breakthrough forces (*inset C*) as obtained from the cluster analysis in *A*.

a scanning speed of 100–400 nm/s. By driving the *z*-piezo at 100–300 Hz only very few PFM curves are taken at each nm in *x* direction. Furthermore, no damage was visible after several scans implying that no permanent damage occurs.

Determination of the sample stiffness

Although the breakthrough distance seems to have no significant dependence on the breakthrough force as shown in Fig. 6, the contact stiffness before breakthrough presented in Fig. 7 on a double logarithmic scale shows a nearly linear increase with increasing breakthrough force. The wider scattering of the data points with increasing contact stiffness reflects the generally reduced sensitivity of an SFM for differences in higher stiffness regimes. The clear trend toward higher contact stiffness at higher forces is in principle agreement with contact theories assuming sphere/elastic half-space geometries, i.e., Hertz (Hertz, 1881), JKR (Johnson et al., 1971), or DMT (Derjaguin et al., 1975) models, where increasing forces lead to larger contact areas and thus larger contact stiffness. However, for reasons of consistency the breakthrough distance should decrease with increasing force—a dependence that could not be observed in our analysis. In this context it should be mentioned that no increasing trend in the breakthrough force or the estimated stiffness could be observed during the measurement, thus a significant flattening of the tip due to the ongoing impacts can be excluded as a reason for latter observation.

To get a magnitude of order estimation of the effective Young modulus and to be able to compare it to data from other groups we used Eq. 2 and a contact radius of $R = 21$ nm (obtained from a calibration on a tip characterization grid), which leads to a mean effective Young modulus of $E = 20$ MPa being in good agreement with the estimated Young modulus $E = 10$–200 MPa of lipid bilayers by Rutkowski et al. (1991). Noteworthy, we use the term ''effective'' Young modulus because the molecular nature of the lipids determines the response measured by the force microscope on the scale of only a few nanometers. Experimentally, no sign of a plastic deformation could be found. The results might as well be interpreted as a tilt of the molecules rather than compression. Furthermore, the thickness of the bilayer (5–6 nm) is too low to neglect the influence of the substrate on the value. In conclusion, we use the term effective Young modulus in agreement with the paper of Franz and Butt to be consistent with literature (Butt and Franz, 2002).

Variation of chain length and headgroup

Breakthrough events could also be detected within the PFM force curves on bilayers of POPC ($T_M = -2.6$°C) and DMPC ($T_M > 23.5$°C) whereas no breakthrough was observed on bilayers of DMPS and DPPS at loads up to 14 nN. The absence of breakthrough events in the case of DMPS ($T_M > 40$°C) and DPPS ($T_M > 50$°C) is presumably due to the fact that those lipids were more closely packed because they are in the gel phase at 25°C and thus withstand external pressure to a higher extend.

As can be seen in the comparison of single breakthrough events in Fig. 8 these are not as featureless as the ones obtained on POPS. On both DMPC and POPC single instabilities might be followed by a short indentation regime, where the tip is indenting a material with stiffness smaller than the stiffness of the intact membrane itself. Subsequently, the tip seems to get into contact with the stiff mica substrate. A third type of breakthrough can be observed on DMPC bilayers (see Fig. 8 *D*) with no indication for any instability. In these ''sliding'' breakthrough events the bilayers do not seem to collapse at any stage of the indentation but are rather smoothly pushed away. Interestingly both DMPC as well as POPC do not show a significant adhesion (data not shown) even after film breakthrough—notably different from the

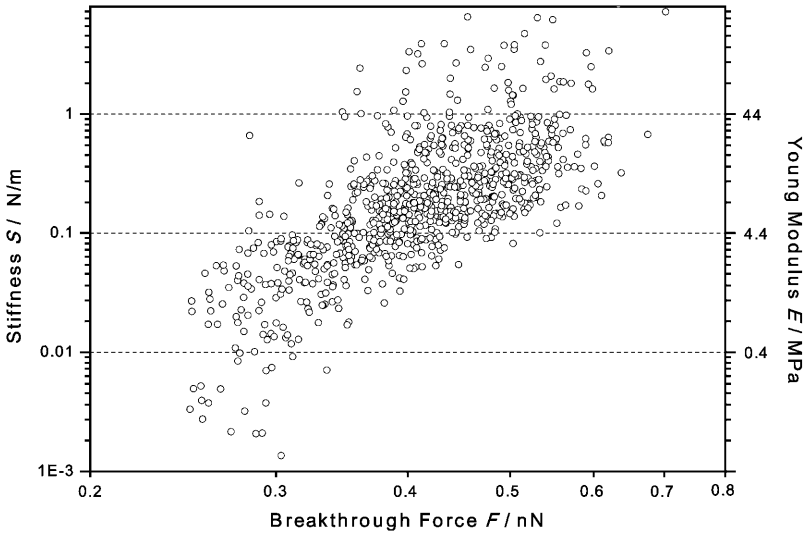

FIGURE 7 Variations of the contact stiffness k_{ss} as calculated from Eq. 1 and the Young modulus E estimated by Eq. 2 as a function of the breakthrough force on a POPS bilayer. The breakthrough events lead to a direct contact with the substrate such that k_{ss} can be interpreted as a measure of the membrane stiffness.

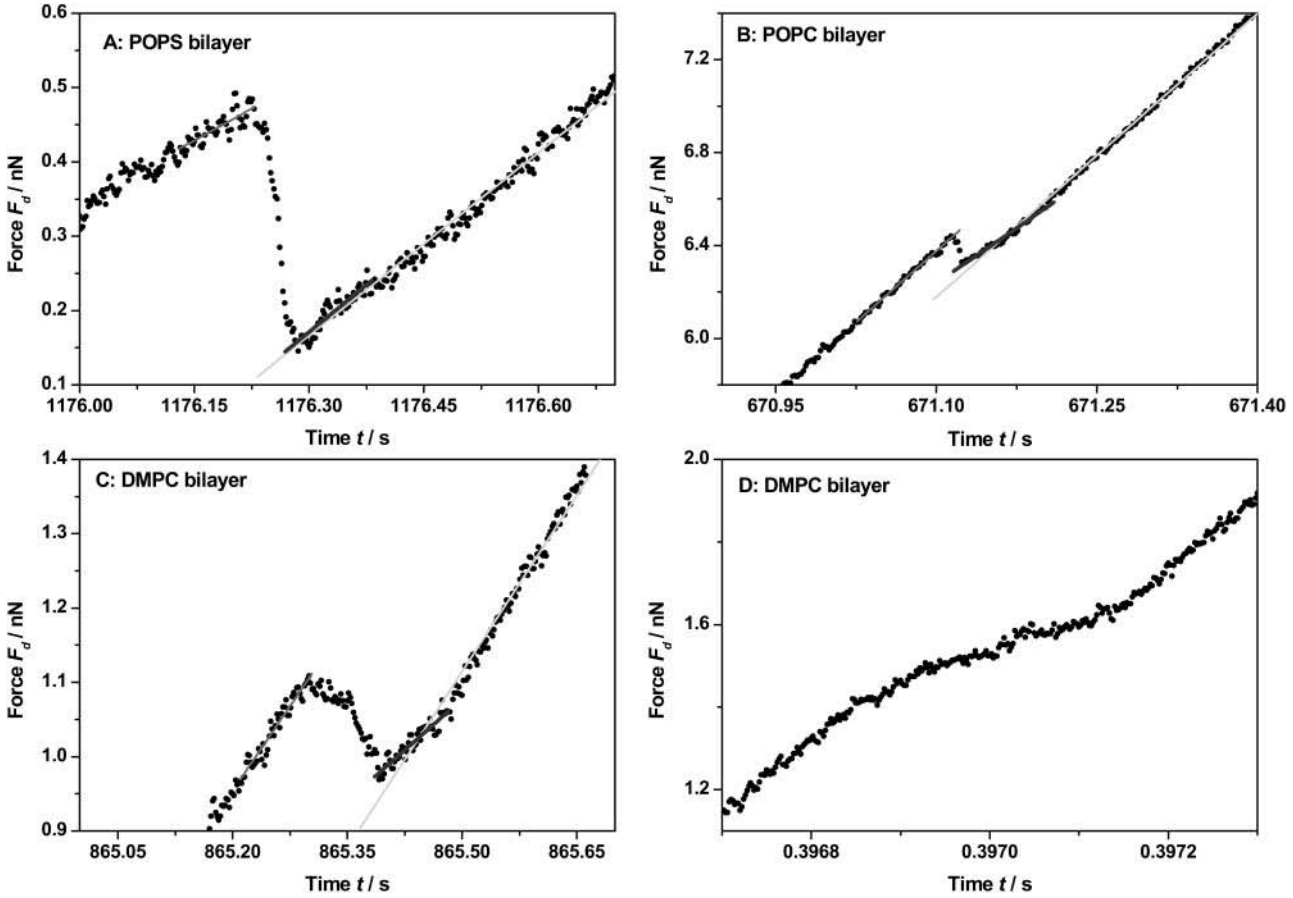

FIGURE 8 Typical PFM force curves measured on lipid bilayers consisting of POPS (*A*), POPC (*B*), and DMPC (*C* and *D*) showing breakthrough events of different mechanism.

observed close relation between adhesion and breakthrough on POPS.

Measuring the mechanical failure of five different bilayer systems made it possible for us to compare both chain length and headgroup dependencies in terms of contact interaction with the SFM tip. The most striking observation was the large difference in the maximum adhesion of PC and PS systems. Being limited to the data obtained from the POPS measurements on the bilayer and the double bilayer alone one would certainly conclude that the adhesion is mostly driven by tip/chain contact: high adhesion was only obtained after breakthrough, which could not be observed in the case of the double bilayer, though exposing the same headgroup toward the tip interface. However, the measurements on the POPC and DMPC systems interfere with this picture of the tip sample interaction. No significant relations between adhesion and breakthrough events were detectable and adhesion is generally much smaller. In summary, one might tend to attribute adhesion of the SFM tip on POPS to parts of the chain groups, which are not exposed to the surface when the film is intact. However, the very different types of breakthrough events of POPC and DMPC might suggest that the mechanism of the penetration followed by mechanical failure is also different compared to POPS and fewer chains might be exposed to the tip after the breakthrough explaining the reduced adhesion.

CONCLUSIONS

The response of solid supported lipid bilayers and multilayers to the indentation by a sharp tip was studied as a function of the number of lamellae, chain length, and headgroup composition. The experiments were performed with a scanning force microscope operating in an optimized pulsed force mode to achieve a high data rate to elucidate the statistical nature of the mechanical failure of model membranes due to the penetration of an SFM tip. One of the major achievements was the implementation of a fast data reduction algorithm enabling the researcher to investigate a large number of force distance curves with respect to breakthrough force and length, adhesion force, and stiffness of the membrane. Because reproducibility is an important issue in scanning force microscopy, this method shows a way out of ambiguous experiments by correlating different mechanical parameters in a cluster analysis. It could be shown that indentation of POPS membranes results in large adhesion

only if mechanical failure of the membrane occurs upon penetrating the membrane. Interestingly, breakthrough events on double bilayers of POPS could not be observed in the measured force regime suggesting that interbilayer stabilization by divalent ions might be responsible for the stabilization of the lamellae.

Furthermore, we were able to show that the mechanical failure of the membranes exhibits a fine structure characteristic for the used lipid. The observation of different types of breakthrough events and accompanying adhesion of POPC, DMPC, and POPS bilayers suggest that the mechanism of the penetration is lipid depending. There is still much work to do to obtain a molecular picture of the failure process as monitored by force distance curves but it will be rewarded by a deeper understanding of physics behind membrane assemblies.

This work was supported by the German Science Foundation (JA 963/1-2).

REFERENCES

Barger, W., D. D. Koleske, K. Feldman, D. Krüger, and R. J. Colton. 1996. Small change—big effect: SPM studies of two-component fatty-acid monolayers. *Polym. Prep.* 37:606–607.

Butt, H. J., and M. Jaschke. 1995. Calculation of thermal noise in atomic force microscopy. *Nanotechnology.* 6:1–7.

Butt, H. J., and V. Franz. 2002. Rupture of molecular thin films observed in atomic force microscopy. I. Theory. *Phys. Rev. E.* 66:031601-1–031601-9.

Cappella, B., and G. Dietler. 1999. Force-distance curves by atomic force microscopy. *Surface Science Reports.* 34:1–104.

Casal, H. L., A. Martin, H. H. Mantsch, F. Paltauf, and H. Hauser. 1987. Infrared studies of fully hydrated unsaturated phosphatidylserine bilayers. *Biochemistry.* 26:7395–7401.

Demel, R. A., F. Paltauf, and H. Hauser. 1987. Monolayer characteristics and thermal behavior of natural and synthetic phosphatidylserines. *Biochemistry.* 26:8659–8665.

Derjaguin, B. B., B. M. Muller, and Y. P. Toporov. 1975. Effect of contact deformation on the adhesion of particles. *J. Colloid Interface Sci.* 53:314–326.

Dufrene, Y. F., W. R. Barger, J. B. D. Green, and G. U. Lee. 1997. Nanometer-scale surface properties of mixed phospholipid monolayers and bilayers. *Langmuir.* 13:4779–4784.

Dufrene, Y. F., T. Boland, J. W. Schneider, W. R. Barger, and G. U. Lee. 1998. Characterization of the physical properties of model biomembranes at the nanometer scale with the atomic force microscope. *Faraday Discuss.* 111:79–94.

Feigenson, G. W. 1986. On the nature of calcium ion binding between phosphatidylserine lamellae. *Biochemistry.* 25:5819–5825.

Feigenson, G. W. 1989. Calcium ion binding between lipid bilayers: the four-component system of phosphatidylserine, phosphatidylcholine, calcium chloride, and water. *Biochemistry.* 28:1270–1278.

Franz, V., S. Loi, H. Müller, E. Bamberg, and H. J. Butt. 2002. Tip penetration through lipid bilayers in atomic force microscopy. *Colloids and Surfaces B. Biointerfaces.* 23:191–200.

Hertz, H. 1881. ber die Berührung fester elastischer Körper. *J. Reine Angew. Math.* 92:156–171.

Janshoff, A., M. Neitzert, Y. Oberdörfer, and H. Fuchs. 2000. Force spectroscopy of molecular systems – single molecule spectroscopy of polymers and biomolecules. *Angew. Chem. Int. Ed.* 39:3212–3237.

Johnson, K. L., K. Kendall, and A. D. Roberts. 1971. Surface energy and the contact of elastic solids. *Proc. R. Soc. Lond. A.* 324:301–313.

Koleske, D. D., W. R. Barger, G. U. Lee, and R. J. Colton. 1997. Scanning probe microscope study of mixed chain-length phase-segregated Langmuir-Blodgett monolayers. *Mat. Res. Soc. Symp. Proc.* 464:377–383.

Krotil, H. U., T. Stifter, H. Waschipky, K. Weishaupt, S. Hild, and O. Marti. 1999. Pulsed force mode: a new method for the investigation of surface properties. *Surface and Interface Analysis.* 27:336–340.

Loi, S., G. Sun, V. Franz, and H. J. Butt. 2002. Rupture of molecular thin films observed in atomic force microscopy. II. Experiment. *Phys. Rev. E.* 66:031602/1–031602/7.

Mattai, J., H. Hauser, R. A. Demel, and G. G. Shipley. 1989. Interactions of metal ions with phosphatidylserine bilayer membranes: effect of hydrocarbon chain unsaturation. *Biochemistry.* 28:2322–2330.

Miyatani, T., M. Horii, A. Rosa, M. Fujihira, and O. Marti. 1997. Mapping of electrical double-layer force between tip and sample surfaces in water with the pulsed-force-mode atomic force microscopy. *Appl. Phys. Lett.* 71:2632–2634.

Miyatani, T., S. Okanoto, A. Rosa, O. Marti, and M. Fujihira. 1998. Surface charge mapping of solid surfaces in water by pulsed-force-mode atomic force microscopy. *Appl. Phys. A.* 66:S349–S352.

Mueller, H., H. J. Butt, and E. Bamberg. 1999. Force measurements on myelin basic protein adsorbed to mica and lipid bilayer surfaces done with the atomic force microscope. *Biophys. J.* 76:1072–1079.

Mueller, H., H. J. Butt, and E. Bamberg. 2000. Adsorption of membrane-associated proteins to lipid bilayers studied with an atomic force microscope: myelin basic protein and cytochrome *c*. *J. Phys. Chem. B.* 104:4552–4559.

Rosa-Zeiser, A., E. Weilandt, S. Hild, and O. Marti. 1997. The simultaneous measurement of elastic, electrostatic and adhesive properties by scanning force microscopy: pulsed-force mode operation. *Meas. Sci. Technol.* 8:1333–1338.

Roux, M., and M. Bloom. 1991. Calcium binding by phosphatidylserine headgroups. *Biophys. J.* 60:38–44.

Rutkowski, C. A., L. M. Williams, T. H. Haines, and H. Z. Cummins. 1991. The elasticity of synthetic phospholipid vesicles obtained by photon correlation spectroscopy. *Biochemistry.* 30:5688–5696.

Schneider, J., Y. F. Dufrene, W. R. Barger, Jr., and G. U. Lee. 2000. Atomic force microscopy image contrast mechanisms on supported lipid bilayers. *Biophys. J.* 79:1107–1118.

Sneddon, I. N. 1965. The relation between load and penetration in the axisymmetric Boussinesq problem for a punch of arbitrary profile. *International Journal of Engineering Science.* 3:47–57.